

# MULTIMODAL TRANSFORMER FOR MATERIAL SEGMENTATION

*Md Kaykobad Reza<sup>1</sup>, Ashley Prater-Bennette<sup>2</sup>, M. Salman Asif<sup>1</sup>*

<sup>1</sup>University of California, Riverside, <sup>2</sup>Air Force Research Laboratory

## ABSTRACT

Leveraging information across diverse modalities is known to enhance performance on multimodal segmentation tasks. However, effectively fusing information from different modalities remains challenging due to the unique characteristics of each modality. In this paper, we propose a novel fusion strategy that can effectively fuse information from different combinations of four different modalities: RGB, Angle of Linear Polarization (AoLP), Degree of Linear Polarization (DoLP) and Near-Infrared (NIR). We also propose a new model named Multi-Modal Segmentation Transformer (MMSFormer) that incorporates the proposed fusion strategy to perform multimodal material segmentation. MMSFormer achieves 52.05% mIoU outperforming the current state-of-the-art on Multimodal Material Segmentation (MCubeS) dataset. For instance, our method provides significant improvement in detecting gravel (+10.4%) and human (+9.1%) classes. Ablation studies show that different modules in the fusion block are crucial for overall model performance. Furthermore, our ablation studies also highlight the capacity of different input modalities to improve performance in the identification of different types of materials. The code and pretrained models will be made available at <https://github.com/csiplab/MMSFormer>.

**Index Terms**— multimodal image segmentation, material segmentation, multimodal fusion, transformer

## 1. INTRODUCTION

Image segmentation [1, 2] methods assign one class label to each pixel in an image. The segmentation map can be used for holistic understanding of objects or context of the scene. Image segmentation can be further divided into different types; examples include semantic segmentation [3, 4], instance segmentation [5, 6], panoptic segmentation [7, 8] and material segmentation [9, 10]. Each of these segmentation tasks are designed to address specific challenges and applications.

Multimodal image segmentation [11, 12] aims to enhance the accuracy and completeness of the task by leveraging diverse sources of information, and potentially leading to a more robust understanding of complex scenes. In contrast to single-modal segmentation, the multimodal approach is

more complex due to the necessity of effectively integrating heterogeneous data from different modalities. Key challenges arise from variations in data quality and attributes, distinct traits of each modality, and need to create models capable of accurately and coherently segmenting with the fused information.

Most of the existing multimodal segmentation methods are designed to work with specific modality pairs, such as RGB-Depth [13, 14, 15], RGB-Thermal [16, 17, 18], and RGB-Lidar [19, 20, 21]. Most of these methods generally do not work well with modality combinations different from the ones used in the original design. Recently, CMX [22] introduced a technique to fuse information from RGB and one other supplementary modality, but it is incapable of fusing more than two modalities at the same time. Some recent models have proposed techniques to fuse more than two modalities [23, 24, 9]. However, they either use very complex fusion strategies [22, 24] or require additional information like semantic labels [9] for performing underlying tasks.

In this paper, we propose a new model for multimodal material segmentation that we call MMSFormer. Our model uses a transformer [25] architecture with a novel fusion block to perform multimodal material segmentation. In particular, our proposed fusion block uses channel attention to combine information across multiple modalities using a small number of linear layers. Such a design provides a simple, lightweight fusion block that can handle an arbitrary number of input modalities.

To test our proposed MMSFormer and fusion block, we focus on multimodal material segmentation using MCubeS dataset [9]. The dataset consists of four different modalities: RGB, angle of linear polarization (AoLP), degree of linear polarization (DoLP) and near-infrared (NIR). We integrate the fusion block with MiX-Transformer [25] to build MMSFormer that provides state-of-the-art performance for multimodal material segmentation [9]. A series of experiments highlight the ability of fusion block to combine different modality combinations, resulting in superior performance compared to current state-of-the-art methods. Ablation studies show that different input modalities assist in identifying different types of materials. Furthermore, as we add new input modalities, overall performance gradually increases.

Main contributions of this paper can be summarized as follows.

- We propose a new multimodal segmentation model called MMSFormer. The model incorporates our proposed fusion block that can fuse information from arbitrary (heterogeneous) combinations of modalities.
- Our model achieves new state-of-the-art performance on multimodal material segmentation (MCubeS) dataset [9]. Furthermore, our method achieves better performance for all modality combinations compared to the current leading models.
- A series of ablation studies show that each module on the fusion block has important contribution towards the overall model performance and each input modality assists in identifying specific types of materials.

Rest of the paper is structured as follows. Section 2 presents a brief review of related work. We describe our model and fusion block in detail in Section 3. Section 4 presents experimental results and ablation studies on multimodal material segmentation task with qualitative and quantitative analysis.

## 2. RELATED WORK

The field of image segmentation has witnessed significant evolution, spurred by advancements in machine learning and computational capabilities. A significant improvement in this evolution came with the inception of fully convolutional networks (FCNs) [26, 27], which revolutionized the field by enabling pixel-wise predictions through the utilization of hierarchical features within convolutional neural networks (CNNs). This led to the development of a variety of CNN based models for different images segmentation tasks. One of the pioneering models that emerged from this era is U-Net [28]. U-Net’s distinctive feature lies in its utilization of skip-connections, which establish direct connections between the lower-resolution feature maps and their corresponding higher-resolution counterparts. DeepLabV3+ [29] introduced dilated convolutions into the encoder, also known as atrous convolutions, allowing the expansion of the receptive field without increasing computational complexity significantly. PSPNet [30] ventured into yet another dimension by introducing global context modules. These modules enable the model to gather information from a wide range of spatial scales, essentially integrating both local and global context into the segmentation process. Collectively, these models ushered in a new era of segmentation techniques, each addressing specific challenges in the field through innovative architectural components.

In recent years, image segmentation field has witnessed a transformative shift with the emergence of transformer-based models. This represents a significant leap forward in the field, as these models utilize the power of attention mechanisms, which have proven to be exceptionally effective in handling complex image segmentation tasks. Some of the notable transformer-based models are PVT (Pyramid Vision

Transformer) [31], SegFormer [25], and Mask2Former [32]. PVT utilizes transformer based design for various computer vision tasks. SegFormer utilizes efficient self-attention and lightweight multilayer perceptron (MLP) decoder for simple and efficient semantic segmentation. Mask2Former uses masked-attention along with pixel decoder and transformer decoder for any segmentation task. Their success demonstrates the capacity of these models to provide state-of-the-art solutions in various segmentation tasks.

In the context of multimodal image segmentation, fusion of data from diverse sources [11] has gained traction as a means to extract richer information and improve accuracy. A variety of models and fusion strategies have been proposed for multimodal segmentation tasks. Notably, the realm of RGB-Depth semantic segmentation has seen several advancements. The FuseNet [14] model integrates depth feature maps into RGB feature maps, while SA-Gate [13] employs Separation-and-Aggregation Gating to mutually filter and recalibrate RGB and depth modalities before fusion. Attention Complementary Module has been proposed by AC-Net [15] that extracts weighted RGB and depth features for fusion. The domain of RGB-Thermal image segmentation has also gained prominence. Recent models include RTFNet [18] which achieves fusion through elementwise addition of thermal features with RGB, RSFNet [16] proposing Residual Spatial Fusion module to blend RGB and Thermal modalities, and EAEFNet [17] utilizing attention interaction and attention complement mechanisms to merge RGB and Thermal features. A number of methods also focus on fusing RGB-Lidar data which include TransFuser [19] that employs Transformer blocks, whereas LIF-Seg [20] relies on coarse feature extraction, offset learning, and refinement for effective fusion.

While the previously mentioned studies focus on specific pairs of modalities, recent research has demonstrated promising results in the fusion of arbitrary modalities. CMX [22] introduces a cross-modal feature rectification module and a feature fusion module to merge RGB features with supplementary modalities. Notably, this fusion technique showcases encouraging outcomes by effectively combining RGB with five distinct modalities individually. For multimodal material segmentation, the MCubeSNet [9] model is proposed, which can seamlessly integrate four different modalities to enhance segmentation accuracy. In the context of arbitrary modal semantic segmentation, CMNeXt [23] introduces Self-Query Hub and Parallel Pooling Mixer modules, offering a versatile approach for fusing diverse modalities. Additionally, HRFuser [24] employs multi-window cross-attention to fuse different modalities at various resolutions, thereby enriching model performance.

These recent advancements underscore the growing interest in exploring flexible and efficient strategies for fusing arbitrary modalities, pushing the boundaries of multimodal image segmentation and its application across diverse scenarios.

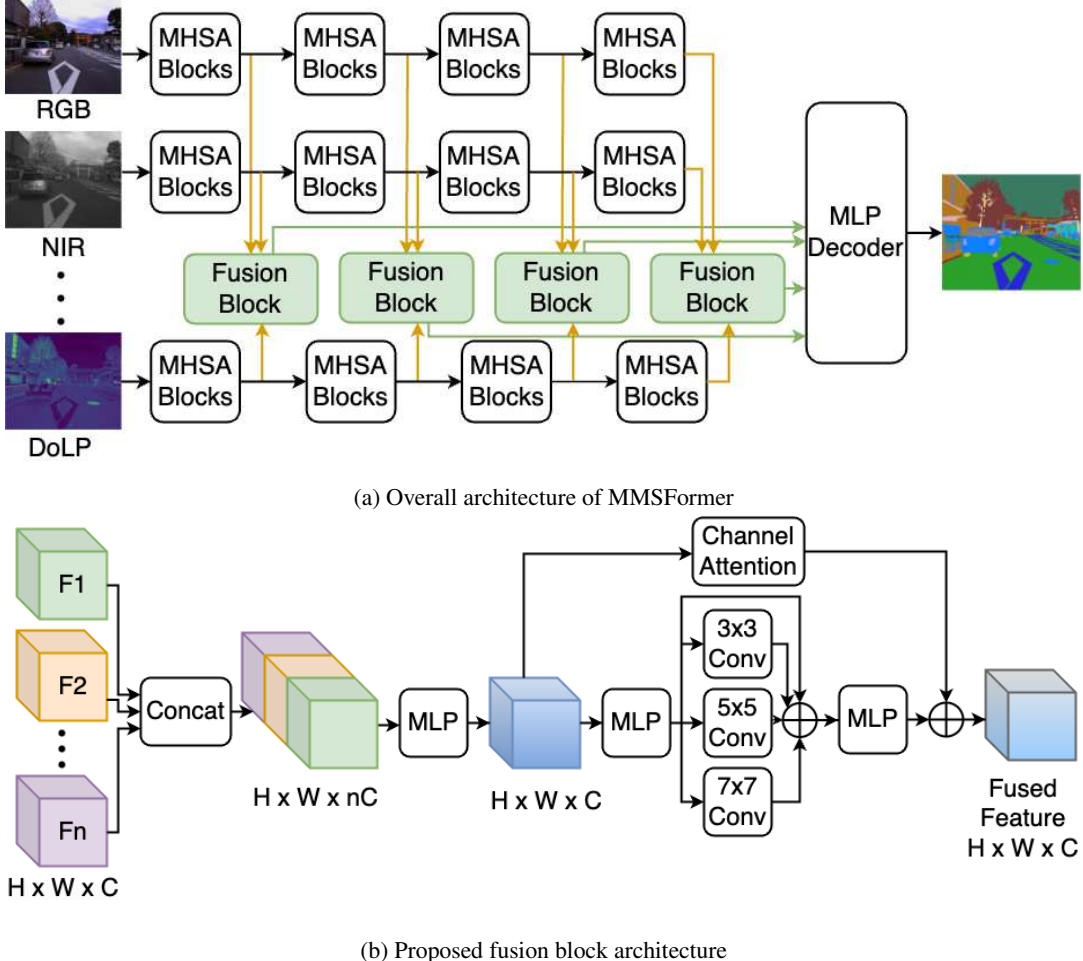


**Fig. 1:** (a) Overall architecture of the proposed MMSFormer model. Each image passes through a modality-specific encoder where we extract hierarchical features. Then we fuse the extracted features using the proposed fusion block and pass the fused features to the decoder for predicting the segmentation maps. (b) Proposed multimodal fusion block. We first concatenate all the features along the channel dimension and pass it through MLP layer to fuse them. Then a mixer layer captures and mixes multi-scale features using parallel convolutions and MLP layers. We use Squeeze and Excitation block as channel attention in the residual connection.

### 3. PROPOSED MODEL

#### 3.1. Model Overview

The overall architecture of our proposed MMSFormer model is shown in Figure 1a. We use modality specific encoders and shared MLP decoder. Modality specific encoders capture distinctive features from each input modality. Then we fuse the extracted features from different modalities with our proposed fusion block shown in Figure 1b and pass the fused features to the MLP decoder to predict the material segmentation labels. We use 4-stage encoders following most of the previous designs [31, 25, 29] to capture pyramidal features from each modality. In particular, we use Mix-Transformer-B2 (MiT-B2) [25] as the encoder. We choose Mix-Transformer for various reasons. First, it can provide multi-scale features without

positional encoding. Second, it uses efficient self-attention that reduces the number of parameters significantly. Third, it also works well with simple and lightweight MLP decoder.

Given a combination of modalities as input, each modality-specific encoder maps the corresponding image into modality-specific multi-scale features as

$$F_m = \text{Encoder}_m(I_m), \quad (1)$$

where  $I_m \in \mathbb{R}^{H \times W \times 3}$  represents image for modality  $m$ . The encoder for  $m$ th modality generates four feature maps of shapes  $(\frac{H}{4} \times \frac{W}{4} \times 64)$ ,  $(\frac{H}{8} \times \frac{W}{8} \times 128)$ ,  $(\frac{H}{16} \times \frac{W}{16} \times 320)$  and  $(\frac{H}{32} \times \frac{W}{32} \times 512)$ , which we represent as  $F_m = \{F_m^1, F_m^2, F_m^3, F_m^4\}$ .

The encoder has a four-stage design, where each stage of the encoder generates feature maps of different shapes. We

use four separate fusion blocks (one corresponding to each encoder stage) to fuse the features from each stage of the encoder. After extracting the features  $F_m$  from all the modalities, we pass them to the fusion block corresponding to the specific stage of the encoder. Each fusion block uses features extracted from all the modalities and fuse them to generate a combined feature representation  $F = \{F^1, F^2, F^3, F^4\}$ .  $F^i$  denotes the fused features at  $i$ th stage that can be represented as

$$F^i = \text{FusionBlock}^i(\{F_m^i\}_m). \quad (2)$$

We pass the combined features  $F$  to the lightweight MLP decoder [25] to predict the material segmentation labels.

### 3.2. Multimodal Fusion Block

The fusion block is responsible for fusing the features extracted from the modality specific encoders. After extracting features  $F_m$  from each modality, we fuse them using the fusion block shown in Figure 1b. We have one fusion block for each of the four encoder stages. For the  $i^{th}$  fusion block, let us assume the input feature maps are given as  $F_m^i \in \mathbb{R}^{H \times W \times C}$  where  $H$ ,  $W$ , and  $C$  can be different for different encoder stages. First, we concatenate the feature maps from  $n$  modalities along the channel dimension to get the combined feature map  $F^i \in \mathbb{R}^{H \times W \times nC}$ . Then we pass the features through an MLP layer that fuses the features by while reducing the channel dimension to  $C$ . Let us denote the resulting features as  $\hat{F}^i \in \mathbb{R}^{H \times W \times C}$ . We represent the operation as

$$\hat{F}^i = \text{MLP}(F_1^i \parallel \dots \parallel F_n^i), \quad (3)$$

$\parallel$  represents concatenation of features along the channel dimension and MLP computes linear combinations along the channel dimension.

Many existing methods have shown that multi-scale features can improve performance for segmentation tasks. For instance, DeepLabV3+ [29] uses dilated convolutions and CMNeXt [23] uses parallel pooling to capture multi-scale features. Inspired by these methods, we design a Mix Feed Forward Network (MixFFN) for capturing and mixing multi-scale features. The MixFFN module consists of two MLP layers having parallel convolution layers in between them. We capture multi-scale features by applying parallel convolutions. Specifically, we apply  $3 \times 3$ ,  $5 \times 5$ , and  $7 \times 7$  convolutions to capture multi-scale features and add them with the residual feature. We apply two MLP layers, one before and one after the parallel convolutions, to mix information in the feature map. Ablation studies show that  $3 \times 3$ ,  $5 \times 5$ , and  $7 \times 7$  convolutions are sufficient for optimal model performance. However, to keep the number of parameter low and the fusion block lightweight, we use depth-wise convolution instead of normal convolution. These steps can be performed as

$$\tilde{F}^i = \text{MLP}(\hat{F}^i), \quad (4)$$

$$F^i = \text{MLP}(\tilde{F}^i + \sum_{k \in \{3,5,7\}} \text{Conv}_{k \times k}(\tilde{F}^i)). \quad (5)$$

Channel attention focuses on learning the importance or relevance of different channels within a feature tensor. The attention modules recalibrate interdependence between channels and allows the model to select the most relevant features or channels while suppressing less important ones. This can lead to more effective feature representations for the underlying task. Channel information play an important role in enhancing model performance. Earlier work [15, 13, 22] used different types of channel attentions to improve model performance for different multimodal segmentation tasks. Motivated by the previous studies, we apply Squeeze-and-Excitation block [33] as channel attention in the residual connection. We represent the final fused feature as

$$F^i = \text{ChannelAttention}(\hat{F}^i) + F^i. \quad (6)$$

Ablation studies show that applying channel attention is crucial to overall model performance and it boosts performance by 0.23% mIoU.

A simple decoder with multiple MLP layers is often sufficient to achieve optimal performance for transformer-based methods. This is because the effective receptive field of the Mix-Transformer encoders are relatively larger than most of the convolutional network-based encoders [25]. To predict the final segmentation map  $\hat{y}$ , we pass the fused features  $F = \{F^1, F^2, F^3, F^4\}$  to an MLP decoder as

$$\hat{y} = \text{MLPDecoder}(F). \quad (7)$$

First, the pyramidal features of different shapes go through an MLP layer to make the channel dimension same for all of them, followed by an upsample operation to unify the spatial dimension. Then they are concatenated and passed through another MLP layer to fuse the features. Finally, the last MLP layer predicts the segmentation maps from the fused features.

In summary, the fusion block extracts and combines useful information from different modality combinations. Each module in the fusion block contributes towards the overall model performance, which we further discuss in the experiment section.

## 4. EXPERIMENTS AND RESULTS

### 4.1. Multimodal Material Segmentation Dataset

Multimodal material segmentation (MCubeS) dataset [9] contains 500 sets of images from 42 street scenes. Each scene has images for four modalities: RGB, angle of linear polarization (AoLP), degree of linear polarization (DoLP), and near-infrared (NIR). The dataset provides annotated ground truth labels for both material and semantic segmentation for every pixel. The dataset is divided training set with 302 image sets, validation set with 96 image sets, and test set with 102 image

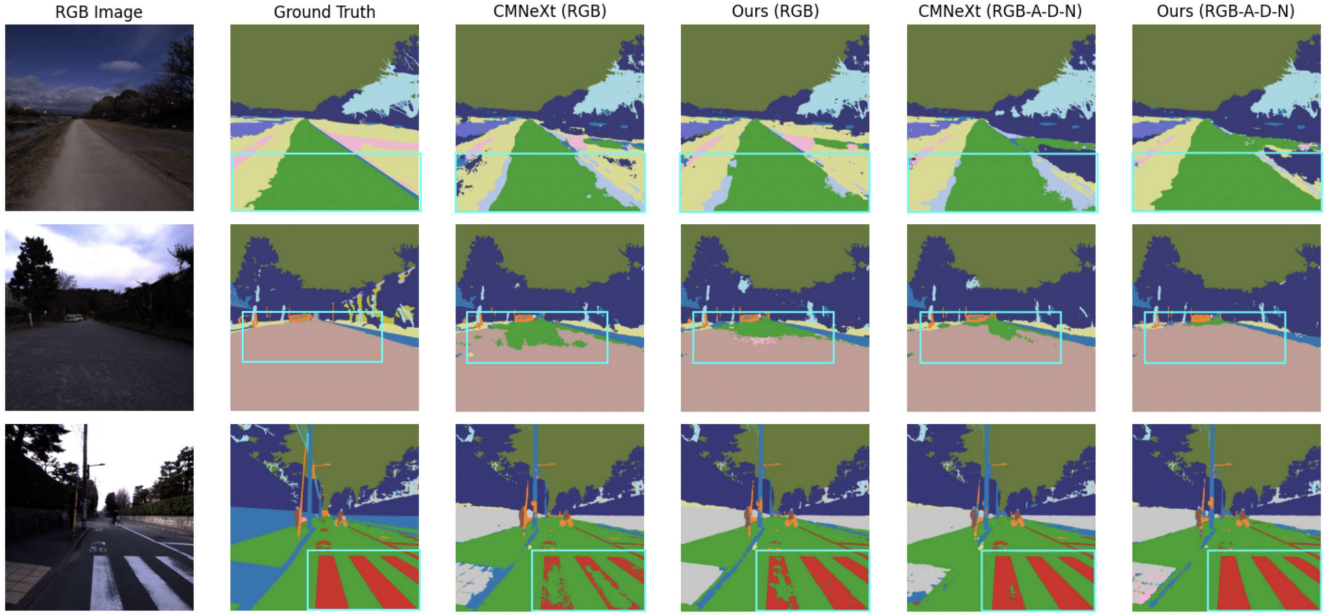


**Fig. 2:** Visualization of results for RGB and all modalities (RGB-A-D-N) prediction with CMNeXt [23] and our proposed MMSFormer. For brevity, we only show the RGB image and Ground Truth material segmentation maps. Our model provides overall better results and correctly identifies asphalt, gravel, and road markings as indicated in the rectangular bounding boxes.

**Table 1:** Performance comparison on Multimodal Material Segmentation (MCubeS) dataset [9]. Here A, D, and N represent angle of linear polarization (AoLP), degree of linear polarization (DoLP), and near-infrared (NIR) respectively.

Method	Modalities	mIoU (%)
DRConv [34]	RGB-A-D-N	34.63
DDF [35]	RGB-A-D-N	36.16
TransFuser [19]	RGB-A-D-N	37.66
DeepLabv3+ [29]	RGB-A-D-N	38.13
MMTM [36]	RGB-A-D-N	39.71
FuseNet [14]	RGB-A-D-N	40.58
MCubeSNet [9]	RGB-A-D-N	42.46
CMNeXt (MiT-B2) [23]	RGB-A-D-N	51.54
<b>MMSFormer (MiT-B2)</b>	RGB-A-D-N	<b>52.05</b>

sets. Each image has  $1224 \times 1024$  pixels and a total of 20 class labels per pixel.

#### 4.2. Implementation Details

To ensure a fair comparison with prior models, we followed the same data preprocessing and augmentation strategies as employed in MCubeSNet [9] and CMNeXt [23]. We used the Mix-Transformer-B2 (MiT-B2) [25] architecture pretrained on the ImageNet [37] dataset as the backbone for our model. Each modality has a separate MiT-B2 [25] encoder, each of

which is initialized with ImageNet [37] pretrained weights. We used a shared MLP decoder from SegFormer [25] and used random initialization for it. Training was conducted for 500 epochs for all the experiments. We trained and evaluated all our models using two NVIDIA RTX 2080Ti GPUs. We used PyTorch for model development.

The initial learning rate was set to  $6 \times 10^{-5}$ , and we utilized a polynomial learning rate scheduler with a power of 0.9 to dynamically adjust the learning rate during training. The first 10 epochs were designated as warm-up epochs with a learning rate of 0.1 times the original rate. For loss computation, we used the cross-entropy loss function. Optimization was performed using the AdamW [38] optimizer with an epsilon value of  $10^{-8}$  and weight decay set to 0.01. A batch size of 4 was employed for all the experiments.

#### 4.3. Comparison with Existing Methods

We conducted a rigorous performance evaluation of our model compared to established baseline models. The comprehensive results are summarized in Table 1. Our model achieves a mean intersection-over-union (mIoU) of 52.05%, surpassing the current state-of-the-art model. Our method also shows significant improvement (more than 9.59%) over all other baseline models available for this dataset. Thus, our model sets new state-of-the-art for the MCubeS dataset.

To further analyze the performance of our model, we conducted a per-class IoU analysis. The results are presented in Table 2. The analysis reveal how our model performs

**Table 2:** Per class % IoU comparison on Multimodal Material Segmentation (MCubeS) [9] dataset. Our proposed *MMSFormer* model shows significant improvement in detecting *Gravel* (+10.4%) and *Human* (+9.1%) classes compared to the current state-of-the-art models while maintaining competitive performance in other classes.

Methods	Asphalt	Concrete	Metal	Road marking	Fabric	Glass	Plaster	Plastic	Rubber	Sand	Gravel	Ceramic	Cobblestone	Brick	Grass	Wood	Leaf	Water	Human	Sky	Mean
MCubeSNet	85.7	42.6	47.0	59.2	12.5	44.3	3.0	10.6	12.7	66.8	67.1	27.8	65.8	36.8	54.8	39.4	73.0	13.3	0.0	94.8	42.9
CMNeXt	84.3	44.9	<b>53.9</b>	<b>74.5</b>	<b>32.3</b>	<b>54.0</b>	<b>0.8</b>	<b>28.3</b>	<b>29.7</b>	67.7	66.5	27.7	68.5	<b>42.9</b>	<b>58.7</b>	<b>49.7</b>	75.4	<b>55.7</b>	18.9	96.5	51.5
<b>MMSFormer</b>	<b>87.7</b>	<b>45.7</b>	52.9	71.2	30.5	51.0	0.4	27.9	25.9	<b>69.7</b>	<b>76.9</b>	<b>28.3</b>	<b>72.0</b>	41.4	56.3	47.2	<b>76.8</b>	54.5	<b>28.0</b>	<b>96.6</b>	<b>52.1</b>

**Table 3:** Performance comparison (% mIoU) on Multimodal Material Segmentation (MCubeS) [9] dataset for different modality combinations.

Modalities	MCubeSNet [9]	CMNeXt [23]	MMSFormer
RGB	33.70	48.16	<b>50.07</b>
RGB-A	39.10	48.42	<b>51.28</b>
RGB-A-D	42.00	49.48	<b>51.57</b>
RGB-A-D-N	42.86	51.54	<b>52.05</b>

on a class-by-class basis. Notably, our model demonstrates a substantial improvement in the detection of gravel and human classes, achieving an increase of 10.4% and 9.1% in IoU, respectively, compared to the current state-of-the-art model. While achieving these notable gains in specific classes, our model also maintained competitive performance across other classes, closely aligning with the current state-of-the-art model.

We show material segmentation results predicted by CMNeXt [23] model and our proposed MMSFormer model in Figure 2. For brevity, we only show RGB images and Ground Truth material segmentation maps in the illustrations. We show RGB only predictions and all modalities (RGB-A-D-N) predictions for both of the models. As shown in the rectangular bounding boxes, our proposed MMSFormer model identifies asphalt, gravel and road marking with greater accuracy than CMNeXt [23] model for both RGB only and all modalities (RGB-A-D-N) predictions.

#### 4.4. Contribution of Different Modalities

A critical aspect of this work involves evaluating the effectiveness of our proposed fusion block in harnessing valuable information from diverse modalities. To analyze this effect, we trained our model with various combinations of modalities. The results are presented in Table 3. Our model exclusively trained on RGB data provided an mIoU score of 50.07%, which 1.91% grater than the current state-of-the-art

model. We observe progressive improvement in performance as we incorporated additional modalities: AoLP, DoLP, and NIR. The integration led to incremental performance gains, with the mIoU increasing from 50.07% to 51.28%, then to 51.57%, and ultimately reaching to 52.05%. These findings serve as a compelling evidence that our fusion approach effectively leverages and fuses valuable information from different combination of modalities, resulting in a notable enhancement in segmentation performance. Furthermore, our model consistently outperforms the current state-of-the-art benchmark across all modality combinations. This consistent superiority underscores the robustness and versatility of our fusion block, demonstrating its ability to adapt and excel regardless of the specific modality combination provided.

#### 4.5. Ablation Study on the Fusion Block

We conducted a series of ablation studies aimed at dissecting the contributions of individual components within the fusion block to the overall model performance. The findings, as detailed in Table 5, shed light on the critical importance of these components. We used all four input modalities during training and testing in these experiments. First, we observed that the absence of channel attention in the residual connection had a negative impact, resulting in a reduction in performance by 0.23%. Moreover, the substitution of channel attention with a  $1 \times 1$  convolution led to a more significant performance drop of 1.47%. This stark contrast underscores the unique capabilities of channel attention in capturing and leveraging crucial information effectively. Additionally, while comparing larger convolution kernel sizes ( $3 \times 3$ ,  $7 \times 7$ , and  $11 \times 11$ ) to the originally employed ( $3 \times 3$ ,  $5 \times 5$ , and  $7 \times 7$ ), we noted a decrease in performance by 0.42%. This result underscores the significance of the carefully chosen convolution kernel sizes within the fusion block.

Furthermore, completely removing the parallel convolutions within the block led to a performance decline of 0.46%, emphasizing their substantial contribution to the overall model’s efficacy. Finally, the MixFFN module, encompassing two MLP layers and the parallel convolutions, was

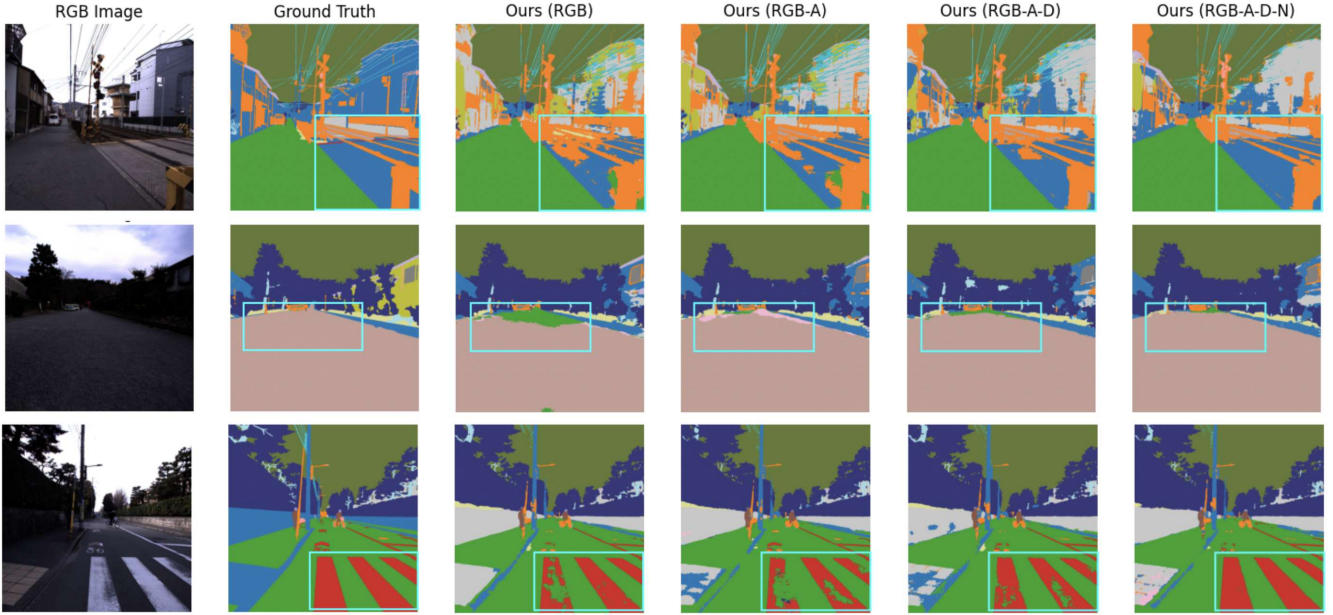


**Fig. 3:** Visualization of results for prediction using different modality combinations of our proposed MMSFormer model. Detection of concrete, gravel and road markings become more accurate as we add more modalities as shown in the rectangular bounding boxes.

found to be exceptionally crucial for the fusion block performance, with a notable drop of 0.81% in its absence. These comprehensive ablation studies collectively underscore the significance of every component within the fusion block, revealing that each module plays a distinct and vital role in achieving the overall performance of our model.

#### 4.6. Ablation Study on Different Modality Combinations

To analyze the contributions of various modalities in the identification of distinct materials, we conducted a series of ablation studies, focusing on per-class IoU for different modality combinations. The insights from these investigations are summarized in Table 4. As we progressively integrate new modalities, a discernible pattern of performance improvement emerges for specific classes, which include asphalt, road marking, sand, gravel, cobblestone and human classes. Particularly noteworthy is the substantial assistance provided by NIR data in classifying sand, gravel, and human categories, leading to significant performance gains in these classes as NIR was added as an additional modality.

Conversely, certain classes such as rubber, grass, and leaf exhibited a gradual performance decline as we introduced additional modalities. This suggests that RGB data alone suffices for accurately identifying these classes, and the inclusion of more modalities potentially introduces noise or redundancy that negatively impacts performance. Moreover, AoLP appears to be instrumental in enhancing the recognition of materials like concrete, metal, fabric, plaster, plastic, ceramic,

and water. Similarly, DoLP is valuable in improving performance for classes like glass, brick, and wood. These findings underscore the relationship between different imaging modalities and the unique characteristics of different types of materials, demonstrating that specific modalities excel in detecting particular classes based on their distinctive traits. Example images are discussed in Figure 3.

In Figure 3, we present some examples to show how adding different modalities help improve performance of segmentation. We show predictions for RGB, RGB-A, RGB-A-D and RGB-A-D-N inputs from our proposed MMSFormer model. As we add new modalities, the predictions become more accurate as shown in the bounding boxes. The illustrations show that the identification of concrete, gravel and road marking becomes more accurate with additional modalities. This also illustrates the capability of the fusion block to effectively fuse information from different modality combinations.

## 5. CONCLUSION

In this paper, we introduce a novel fusion block designed to combine useful information from various modality combinations. We also propose a new model called MMSFormer that integrates the proposed fusion block to accomplish multimodal material segmentation task. Experimental results illustrate the model’s capability to efficiently fuse features from four distinct modalities, leading to a new state-of-the-art performance on the Multimodal Material Segmentation

**Table 4:** Per class % IoU comparison on Multimodal Material Segmentation (MCubeS) [9] dataset for different modality combinations. As we add modalities incrementally, overall performance increases gradually. This table also shows that specific modality combinations assist in identifying specific types of materials better.

Modalities	Asphalt	Concrete	Metal	Road marking	Fabric	Glass	Plaster	Plastic	Rubber	Sand	Gravel	Ceramic	Cobblestone	Brick	Grass	Wood	Leaf	Water	Human	Sky	Mean
RGB	86.0	44.3	52.1	70.1	31.5	54.5	0.2	23.0	<b>28.6</b>	62.8	62.4	29.2	70.2	43.7	<b>60.8</b>	47.3	<b>77.3</b>	46.1	14.9	96.5	50.1
RGB-A	86.8	45.8	<b>54.7</b>	69.6	<b>35.7</b>	53.8	<b>2.1</b>	<b>30.6</b>	28.1	65.2	63.8	<b>30.1</b>	67.6	42.5	59.8	46.1	76.6	<b>56.8</b>	13.3	96.5	51.3
RGB-A-D	87.0	<b>47.5</b>	54.4	70.6	33.7	<b>55.2</b>	0.5	26.7	27.5	62.6	66.9	28.2	69.9	<b>45.2</b>	58.4	<b>47.6</b>	75.7	56.6	20.7	96.5	51.6
RGB-A-D-N	<b>87.7</b>	45.7	52.9	<b>71.2</b>	30.5	51.0	0.4	27.9	25.9	<b>69.7</b>	<b>76.9</b>	28.3	<b>72.0</b>	41.4	56.3	47.2	76.8	54.5	<b>28.0</b>	<b>96.6</b>	<b>52.1</b>

**Table 5:** Ablation study of the *Fusion Block* on Multimodal Material Segmentation (MCubeS) [9] dataset. All the four input modalities were used during training and testing. The table shows the contribution of different modules in fusion block in overall model performance.

Structure	% mIoU (Change)
MMSFormer (MiT-B2)	<b>52.05</b>
- without channel attention	51.82 <i>(-0.23)</i>
- 1x1 conv instead of channel attention	50.58 <i>(-1.47)</i>
- with 3x3, 7x7 & 11x11 convolutions	51.63 <i>(-0.42)</i>
- without parallel convolutions	51.59 <i>(-0.46)</i>
- without MixFFN	51.24 <i>(-0.81)</i>

(MCubeS) dataset. Experiments also show that the fusion block can extract useful information from different modality combinations which helps the model to consistently outperform current state-of-the-art model. Performance increases gradually as we add new modalities. Several ablation studies further highlight how different components of the fusion block contribute to the overall model performance. Ablation studies also reveal that different modalities assist in identifying different types of materials. Future work may include investigating the model’s performance with modalities beyond the four explored in this paper and other multimodal segmentation tasks.

## 6. REFERENCES

- [1] Shervin Minaee, Yuri Boykov, Fatih Porikli, Antonio Plaza, Nasser Kehtarnavaz, and Demetri Terzopoulos, “Image segmentation using deep learning: A survey,” *IEEE transactions on pattern analysis and machine intelligence*, vol. 44, no. 7, pp. 3523–3542, 2021.
- [2] Heng-Da Cheng, X. H. Jiang, Ying Sun, and Jingli Wang, “Color image segmentation: advances and prospects,” *Pattern recognition*, vol. 34, no. 12, pp. 2259–2281, 2001.
- [3] Yanming Guo, Yu Liu, Theodoros Georgiou, and Michael S Lew, “A review of semantic segmentation using deep neural networks,” *International journal of multimedia information retrieval*, vol. 7, pp. 87–93, 2018.
- [4] Panqu Wang, Pengfei Chen, Ye Yuan, Ding Liu, Zehua Huang, Xiaodi Hou, and Garrison Cottrell, “Understanding convolution for semantic segmentation,” in *2018 IEEE winter conference on applications of computer vision (WACV)*. Ieee, 2018, pp. 1451–1460.
- [5] Abdul Mueed Hafiz and Ghulam Mohiuddin Bhat, “A survey on instance segmentation: state of the art,” *International journal of multimedia information retrieval*, vol. 9, no. 3, pp. 171–189, 2020.
- [6] Wenchao Gu, Shuang Bai, and Lingxing Kong, “A review on 2d instance segmentation based on deep neural networks,” *Image and Vision Computing*, vol. 120, pp. 104401, 2022.
- [7] Alexander Kirillov, Kaiming He, Ross Girshick, Carsten Rother, and Piotr Dollár, “Panoptic segmentation,” in *Proceedings of the IEEE/CVF conference on computer vision and pattern recognition*, 2019, pp. 9404–9413.
- [8] Omar Elharrouss, Somaya Ali Al-Maadeed, Nandhini Subramanian, Najmath Ottakath, Noor Almaadeed, and Yassine Himeur, “Panoptic segmentation: A review,” *ArXiv*, vol. abs/2111.10250, 2021.
- [9] Yupeng Liang, Ryosuke Wakaki, Shohei Nobuhara, and Ko Nishino, “Multimodal material segmentation,” in *Proceedings of the IEEE/CVF Conference on Computer Vision and Pattern Recognition (CVPR)*, June 2022, pp. 19800–19808.
- [10] Paul Upchurch and Ransen Niu, “A dense material segmentation dataset for indoor and outdoor scene parsing,” in *European Conference on Computer Vision*. Springer, 2022, pp. 450–466.
- [11] Yifei Zhang, Désiré Sidibé, Olivier Morel, and Fabrice Mériaudeau, “Deep multimodal fusion for semantic image segmentation: A survey,” *Image and Vision Computing*, vol. 105, pp. 104042, 2021.
- [12] Zhe Guo, Xiang Li, Heng Huang, Ning Guo, and Quanzheng Li, “Deep learning-based image segmentation on multimodal medical imaging,” *IEEE Transactions on Radiation and Plasma Medical Sciences*, vol. 3, no. 2, pp. 162–169, 2019.
- [13] Xiaokang Chen, Kwan-Yee Lin, Jingbo Wang, Wayne Wu, Chen Qian, Hongsheng Li, and Gang Zeng, “Bi-

directional cross-modality feature propagation with separation-and-aggregation gate for rgb-d semantic segmentation,” in *European Conference on Computer Vision (ECCV)*, 2020, pp. 561–577.

[14] C. Hazirbas, L. Ma, C. Domokos, and D. Cremers, “Fusenet: incorporating depth into semantic segmentation via fusion-based cnn architecture,” in *Asian Conference on Computer Vision*, November 2016.

[15] Xinxin Hu, Kailun Yang, Lei Fei, and Kaiwei Wang, “Acnet: Attention based network to exploit complementary features for rgbd semantic segmentation,” in *IEEE International Conference on Image Processing (ICIP)*, 2019, pp. 1440–1444.

[16] Ping Li, Junjie Chen, Binbin Lin, and Xianghua Xu, “Residual spatial fusion network for rgb-thermal semantic segmentation,” *arXiv preprint arXiv:2306.10364*, 2023.

[17] Mingjian Liang, Junjie Hu, Chenyu Bao, Hua Feng, Fuqin Deng, and Tin Lun Lam, “Explicit attention-enhanced fusion for rgb-thermal perception tasks,” *IEEE Robotics Autom. Lett.*, vol. 8, no. 7, pp. 4060–4067, 2023.

[18] Yuxiang Sun, Weixun Zuo, and Ming Liu, “RTFNet: RGB-Thermal Fusion Network for Semantic Segmentation of Urban Scenes,” *IEEE Robotics and Automation Letters*, vol. 4, no. 3, pp. 2576–2583, July 2019.

[19] Aditya Prakash, Kashyap Chitta, and Andreas Geiger, “Multi-modal fusion transformer for end-to-end autonomous driving,” in *Proceedings of the IEEE/CVF Conference on Computer Vision and Pattern Recognition*, 2021, pp. 7077–7087.

[20] Lin Zhao, Hui Zhou, Xinge Zhu, Xiao Song, Hongsheng Li, and Wenbing Tao, “Lif-seg: Lidar and camera image fusion for 3d lidar semantic segmentation,” *IEEE Transactions on Multimedia*, pp. 1–11, 2023.

[21] J. Li, H. Dai, H. Han, and Y. Ding, “Mseg3d: Multi-modal 3d semantic segmentation for autonomous driving,” in *2023 IEEE/CVF Conference on Computer Vision and Pattern Recognition (CVPR)*, Los Alamitos, CA, USA, jun 2023, pp. 21694–21704, IEEE Computer Society.

[22] Jiaming Zhang, Huayao Liu, Kailun Yang, Xinxin Hu, Ruiping Liu, and Rainer Stiefelhagen, “Cmx: Cross-modal fusion for rgb-x semantic segmentation with transformers,” *IEEE Transactions on Intelligent Transportation Systems*, 2023.

[23] Jiaming Zhang, Ruiping Liu, Hao Shi, Kailun Yang, Simon Reiß, Kunyu Peng, Haodong Fu, Kaiwei Wang, and Rainer Stiefelhagen, “Delivering arbitrary-modal semantic segmentation,” in *Proceedings of the IEEE/CVF Conference on Computer Vision and Pattern Recognition*, 2023, pp. 1136–1147.

[24] Tim Broedermann, Christos Sakaridis, Dengxin Dai, and Luc Van Gool, “Hrfuser: A multi-resolution sensor fusion architecture for 2d object detection,” in *IEEE International Conference on Intelligent Transportation Systems (ITSC)*, 2023.

[25] Enze Xie, Wenhui Wang, Zhiding Yu, Anima Anandkumar, Jose M Alvarez, and Ping Luo, “Segformer: Simple and efficient design for semantic segmentation with transformers,” in *Neural Information Processing Systems (NeurIPS)*, 2021.

[26] Jonathan Long, Evan Shelhamer, and Trevor Darrell, “Fully convolutional networks for semantic segmentation,” in *Proceedings of the IEEE conference on computer vision and pattern recognition*, 2015, pp. 3431–3440.

[27] Huihai Wu, Junge Zhang, Kaiqi Huang, Kongming Liang, and Yizhou Yu, “Fastfcn: Rethinking dilated convolution in the backbone for semantic segmentation,” *arXiv preprint arXiv:1903.11816*, 2019.

[28] Olaf Ronneberger, Philipp Fischer, and Thomas Brox, “U-net: Convolutional networks for biomedical image segmentation,” in *Medical Image Computing and Computer-Assisted Intervention—MICCAI 2015: 18th International Conference, Munich, Germany, October 5–9, 2015, Proceedings, Part III* 18. Springer, 2015, pp. 234–241.

[29] Liang-Chieh Chen, Yukun Zhu, George Papandreou, Florian Schroff, and Hartwig Adam, “Encoder-decoder with atrous separable convolution for semantic image segmentation,” in *Proceedings of the European conference on computer vision (ECCV)*, 2018, pp. 801–818.

[30] Hengshuang Zhao, Jianping Shi, Xiaojuan Qi, Xiaogang Wang, and Jiaya Jia, “Pyramid scene parsing network,” in *Proceedings of the IEEE conference on computer vision and pattern recognition*, 2017, pp. 2881–2890.

[31] Wenhui Wang, Enze Xie, Xiang Li, Deng-Ping Fan, Kaitao Song, Ding Liang, Tong Lu, Ping Luo, and Ling Shao, “Pyramid vision transformer: A versatile backbone for dense prediction without convolutions,” in *Proceedings of the IEEE/CVF international conference on computer vision*, 2021, pp. 568–578.

[32] Bowen Cheng, Ishan Misra, Alexander G Schwing, Alexander Kirillov, and Rohit Girdhar, “Masked-attention mask transformer for universal image segmentation,” in *Proceedings of the IEEE/CVF conference on computer vision and pattern recognition*, 2022, pp. 1290–1299.

[33] Jie Hu, Li Shen, and Gang Sun, “Squeeze-and-excitation networks,” in *Proceedings of the IEEE conference on computer vision and pattern recognition*, 2018, pp. 7132–7141.

[34] Jin Chen, Xijun Wang, Zichao Guo, Xiangyu Zhang, and Jian Sun, “Dynamic region-aware convolution,” in *Proceedings of the IEEE/CVF conference on computer vision and pattern recognition*, 2021, pp. 8064–8073.

[35] Jingkai Zhou, Varun Jampani, Zhixiong Pi, Qiong Liu, and Ming-Hsuan Yang, “Decoupled dynamic filter networks,” in *Proceedings of the IEEE/CVF Conference on Computer Vision and Pattern Recognition*, 2021, pp. 6647–6656.

[36] Hamid Reza Vaezi Joze, Amirreza Shaban, Michael L Iuzzolino, and Kazuhito Koishida, “Mmtm: Multimodal transfer module for cnn fusion,” in *Proceedings of the IEEE/CVF conference on computer vision and pattern recognition*, 2020, pp. 13289–13299.

[37] Jia Deng, Wei Dong, Richard Socher, Li-Jia Li, Kai Li, and Li Fei-Fei, “Imagenet: A large-scale hierarchical image database,” in *2009 IEEE Conference on Computer Vision and Pattern Recognition*, 2009, pp. 248–255.

[38] Ilya Loshchilov and Frank Hutter, “Decoupled weight decay regularization,” in *International Conference on Learning Representations*, 2019.